AUT Journal of Mechanical Engineering

AUT J. Mech. Eng., 3(1) (2019) 53-62
DOI: 10.22060/ajme.2018.14440.5729

New Design and Analysis of Diesel Exhaust Manifold to Control Thermal Gradient

M.R. Assari*, A. Ebn-Abbas, S. Adeli

Department of Mechanical Engineering, Jundi-Shapur University of Technology, Dezful, Iran

ABSTRACT: Optimization and design of new configurations in the field of engineering became faster and more accurate by improving three dimension modeling software and computational fluid dynamics methods. Exhaust manifold of the marine diesel engine, which transfers hot gases from cylinders to the turbocharger, has a problem with extreme thermal gradients and crack creation which cause coolant leakage to the combustion gases paths. Thus, the turbocharger and engine operation will be interrupted. In cooling systems, the main goal is to achieve uniform thermal distribution. In order to improve the heat transfer and prevent crack occurrence at the detected critical points, new configurations in geometrics design for exhaust manifold were studied in this paper.

Two Proposed configurations were designed in the Solidworks modeling software. Flow simulation of thermal analysis was performed in ANSYS CFX by using Rensselaer Polytechnic Institute wall boiling model for subcooled boiling at the low pressure. Analysis indicated the single channel configuration, performed by removing output-separating wall on hot gases side, provide more uniform temperature distribution in the manifold body Results showed the correct operation of new manifold geometry that reduces the maximum temperature of the body up to 27.36% and controls the extreme (amount of) thermal gradients and risk of crack occurrence.

Review History:

Received: 16 May 2018
Revised: 19 September 2018
Accepted: 19 December 2018
Available Online: 11 February 2019

Keywords:

Exhaust manifold
Subcooled boiling
Computational fluid dynamics
Crack creation
Rensselaer Polytechnic Institute separation model
Water jacket

1- Introduction

Recent studies on Internal Combustion (IC) engines have led to increase their efficiency. Therefore, increasing the heat generation is an inevitable result in engines. Researchers focused on the optimal design of the engine cooling system [1]. These following objectives were generally considered in the design of engine cooling systems and coolant flow path [2]:

- Keep wall temperature and other engine components with acceptable limits to prevent thermal stress failure.
- Minimizing the pressure drop.
- Prevention of stagnation point in the coolant flow path.

The optimal design of the cooling system should be able to control engine components temperature under various operating conditions and keep the temperature stable and uniform. Therefore, the amount of absorbed heat and thermal gradients controlling by coolant fluid is important. Experimental investigation of cooling jacket complex path is time-consuming and extremely difficult. Using an alternative and practical approach in this field is worthful. Computational Fluid Dynamics (CFD) and its abilities and computational power of new computers cause improvements in engine research and achieving optimized model is easier. Karl and Feldhaus [3] emphasized applications and capabilities of CFD methods. That is why the research and development department of engine manufacturers is moving towards software simulation and analysis. They used Flowmaster, which includes all systems for simulation of flow in cooling circuit. Their goals were to achieve thermostat valve behavior, exhaust gas temperature, optimal ratio for combination water and glycol in the cooling system, and required power for its pumping system in different conditions of engine operation.

In heavy industries like marine which mechanical power at the high level is necessary, diesel engines are promising due to their efficiency and high pressure ratio. These engines have relatively high temperature and pressure in exhaust gases [4]. In order to improve the efficiency and reduce the fuel consumption, hot gases power were used to move the turbocharger in 900-1000 oC . Hence, the manifold plays a vital role to deliver hot gases from cylinder to the turbocharger. Kanawade and Siras [5] used STAR CCM+ to optimize the manifold geometry and decreased 26% flow losses and pressure drop in comparison with the primary model. Strict standards for marines states that the maximum allowable temperature in the engine room is 60-70oC. Therefore, the manifold body should be cooled with the cooling system and seawater [6].

Due to the high temperature of hot gases, the cooling fluid experiences the heat transfer process in the nuclear boiling region and the convection type of heat transfer. In order to suggest an alternative model it should be noted that if the heat transfers process changes into the film-boiling region, the creation of vapor layer in the vicinity prevents appropriate heat transfer in the wall.

There are several models to analyze the heat transfer processes considering the boiling phenomenon: Boundary layer turbulence model, Micro-layer separation model, and Rensselaer Polytechnic Institute (RPI) wall boiling model. From these models, the most credible one for analyzing the current issue is RPI model, which based on the separation of wall heat flux. The model first introduced by Bowring [7] in RPI, further developed by Podowski [8], and became the

Corresponding author, E-mail: assari.mr@gmail.com

main criterion of discretization.

The aim of most studies was to achieve the uniform cooling method and prevent the occurrence of phenomena such as body distortion and cavitation. Shingare [9] used Ansys-Fluent to find the optimal ratio for the combination of water and glycol as a coolant fluid of four-cylinder diesel engine. A combination with equal ratio was kept engine body in stable thermal conditions. Romanov [10] achieved the same goals, investigated the effect of changing the location of the coolant fluid inlet, the places where the coolant penetrates into the jacket, on the distribution of temperature on the cylinder body. For this purpose, they used two-phase flow analysis approach and divided domain into three parts: coolant, body, and hot combustible gases. Rising heat transfer coefficient in boiling was one of the results of this phenomenon. Mohammadi [11] used two-phase flow analysis approach for simulation of a diesel engine water jacket. They validated the simulation results with the results of laboratory studies. Contours of velocity indicated that nucleate boiling occurred around the poppet valve of exhaust gas was due to the reduction of coolant flow cross-section and its velocity. By extracting a volumetric fraction of vapor, they were assured of the correct function of the water jacket.

Paratwar and Hulwan [12] studied the cooling system of a cylinder head in a 6-cylinder engine. Their simulation result was verified by experimental data. They observed hot spots in geometry, which led to extreme temperature gradients. They proposed optimized geometry by creating new paths for coolant fluid. They succeeded in reducing the temperature of hot spots between 7-10oC also decreasing pressure drops across the water jacket.

Punekar and Das [2] used Chen's correlation to study subcooled nucleate boiling and near wall bubble dynamics in IC engine cooling jackets. The volume fraction of vapor showed that all the vapor, which formed in lower passages of coolant fluid, quickly move up due to the floating force. The maximum volume fraction of the vapor did not exceed 10%, which indicates that in the most critical areas of geometry, the boiling process is within the permitted range and has not entered to film boiling range. They emphasized the importance of considering the two-phase flow by comparing the heat transfer results obtained from single-phase and two-phase solution.

Studies on the primary geometry of manifold indicated hot spots and extreme thermal gradient on output separator wall because of the non-uniform cooling process. Laboratory tests also detected that the crack occurrence at the predicted point in the simulation.

In this study, the thermal-fluid analysis of proposed geometries with consideration of the boiling phenomenon was investigated. Subcooled boiling usually occurs when there is local boiling at superheated wall surface by high heat fluxes, even though the bulk flow has not reached the saturated temperature. Results represent in temperature contours over whole geometry.

The suggestion of two alternative geometries was based on the investigation of primary geometry and its problems (see Fig. 1)

The main goal of this study is to achieve better thermal behavior of manifold. These models will be analyzed by applying the engine operating conditions and the appropriate computational model. The Analysis results are presented as thermal distribution contours in different configurations to make the results comparable. After achieving better configuration, without any extra cost and time consumption to build laboratory models, the results are presented to the industrial unit to build a better and assured alternative manifold configuration.

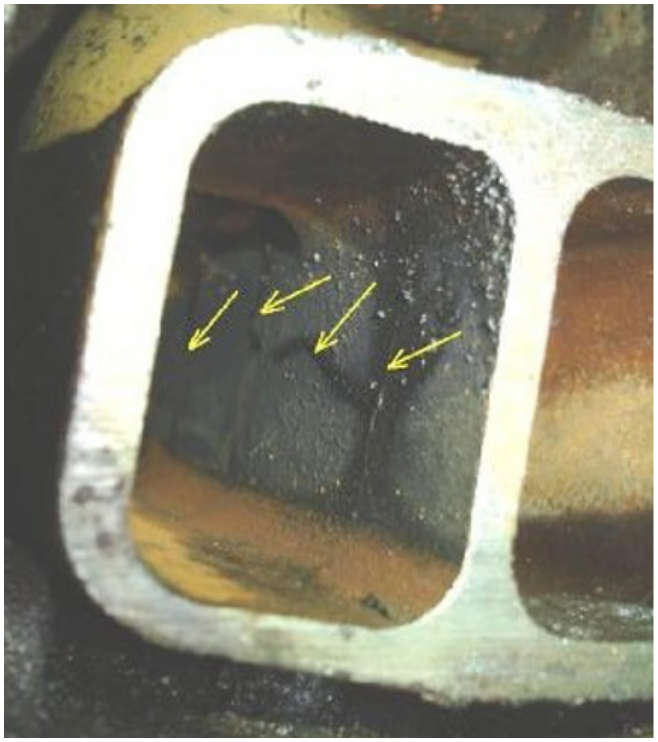

Fig. 1. Industrial center Laboratory tests detect crack occurrence on output separator wall

Two Proposed configurations were designed in the Solidworks modeling software (see Fig. 2b and 2c). Designing alternative configurations was in order to prevent the formation of hot spots and well controlled temperature distribution. For these purpose two strategies as single and dual channel configuration was implemented. First, as dual channel model, creating a path for coolant fluid through the output separating wall in the vicinity of the maximum temperature point on the manifold body in order to absorb heat and control the temperature of this point (see Fig. 2b). Next, as a single channel configuration, removing a part of geometry where hotspot occurred with considering proper function of the manifold. It was output separating wall on the hot gas side, the place where the crack was detected (see Fig. 2c).

2- Modeling

Subcooled boiling flow in the cooling passages of the exhaust manifold of diesel engine describes by Two-fluid Eulerian-Eulerian. Mass, momentum, and energy Equations have been written separately for different phases; and, because of the dispersed phase of vapor bubbles, is the liquid is treated as the continuous phase. Liquid and gaseous phases continuity equations are:

$$\frac{\partial\left(\rho_l \alpha_l\right)}{\partial t}+\nabla.\left(\rho_l \alpha_l \overrightarrow{u_l}\right)=\Gamma_{\mathrm{lg}} \tag{1}$$

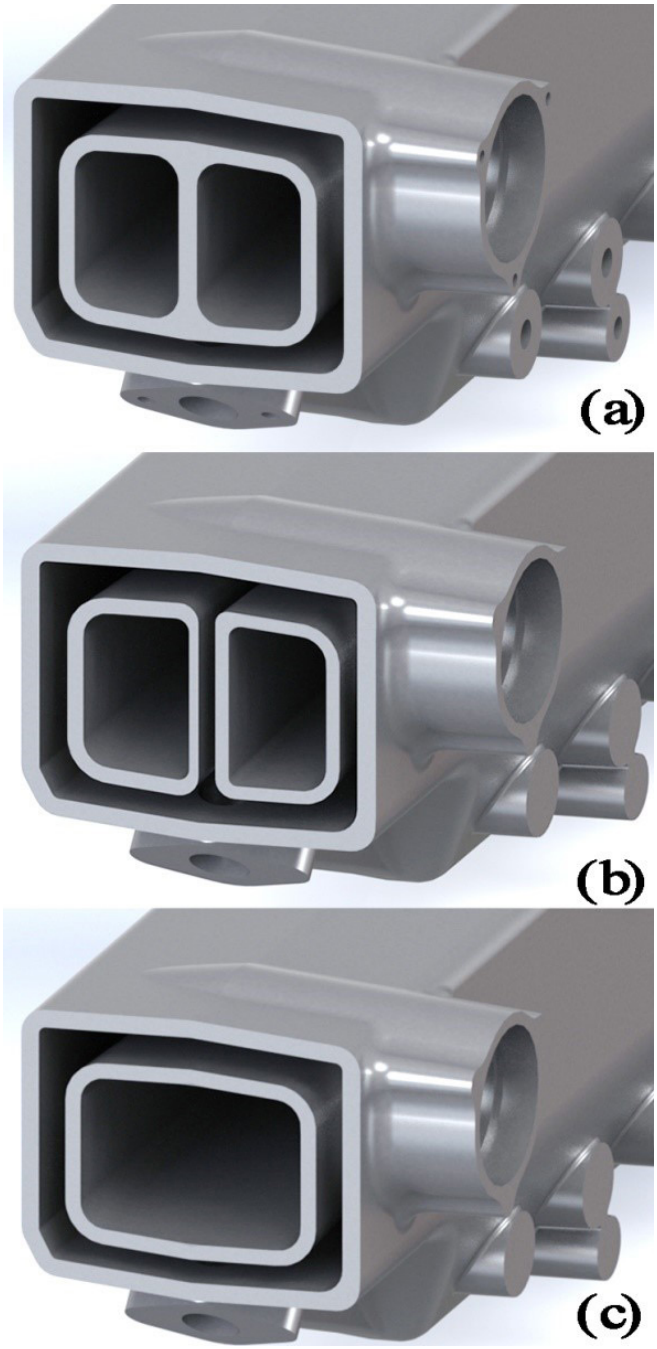

Fig. 2. (a) primary geometry, (b) First proposed configuration (Dual Channel), (c) second proposed configuration (Single channel)

$$\frac{\partial\left(\rho_g \alpha_g f_i\right)}{\partial t}+\nabla.\left(\rho_g \alpha_g \overrightarrow{u_g} f_i\right)=S_i-f_i \Gamma_{lg} \tag{2}$$

For liquid and gaseous phase momentum equations [13]:

$$\begin{aligned}&\frac{\partial\left(\rho_l \alpha_l \overrightarrow{u_l}\right)}{\partial t}+\nabla.\left(\rho_l \alpha_l \overrightarrow{u_l} \times \overrightarrow{u_l}\right)= \\ &\left(-\alpha_l \nabla p\right)+\nabla.\left(\alpha_l \mu_l\left(\nabla u_l+\left(\nabla u_l{}^T\right)\right)\right) \\ &+\Gamma_{lg} \overrightarrow{u_g}-\Gamma_{lg} \overrightarrow{u_l}+\overrightarrow{F_{lg}}\end{aligned} \tag{3}$$

$$\begin{aligned}&\frac{\partial\left(\rho_g \alpha_g \overrightarrow{u_g}\right)}{\partial t}+\nabla.\left(\rho_g \alpha_g \overrightarrow{u_g} \times \overrightarrow{u_g}\right)=\left(-\alpha_l \nabla p\right) \\ &+\nabla.\left(\alpha_g \mu_g\left(\nabla u_g+\left(\nabla u_g{}^T\right)\right)\right)-\Gamma_{lg} \overrightarrow{u_g}+\Gamma_{gl} \overrightarrow{u_l}-\overrightarrow{F_{lg}}\end{aligned} \tag{4}$$

Liquid phase of Energy equation:

$$\begin{aligned}&\frac{\partial\left(\rho_l \alpha_l h_l\right)}{\partial t}+\nabla.\left(\rho_l \alpha_l \overrightarrow{u_l} h_l-\lambda_l \alpha_l \nabla T_l\right) \\ &=\Gamma_{lg} h_g-\Gamma_{gl} h_l+\mathrm{Q}_l\end{aligned} \tag{5}$$

The flow regime through the engine cooling passage is mainly turbulent and due to the low-density criteria, the motion of the dispersed vapor phase is commonly assumed dependent on the continuous liquid phase [14]. In this article the Shear Stress Transport (SST) turbulence model applies to the continuous liquid phase, and a disperse phase zero-equation model to the vapor phase [15].
Furthermore, according to the large bubbles and fluctuating wakes, the boiling flow generates an additional liquid turbulence viscosity term μ_l^b modeled using Sato's eddy viscosity model [16]. So, the viscosity is shown as:

$$\mu_l^{eff}=\mu_l+\mu_l^{turb}+\mu_l^b \tag{6}$$

μ_l^{eff} shows the effective viscosity in momentum and energy equations, μ_l is molecular viscosity, μ_l^{turb} is shear-induced turbulence viscosity, μ_l^b is defined as:

$$\mu_l^b=C_{\mu b} \rho_l \alpha d_b\left|\overrightarrow{u_g}-\overrightarrow{u_l}\right| \tag{7}$$

The coefficient $C_{\mu b}$ is set to 0.6 the default value. The near wall region is assumed to follow the logarithmic law in single-phase state.
The subcooled boiling flow of inter-phase momentum transfer is usually modeled with the following interfacial forces: drag force F_D and non-drag force such as lift force F_L turbulent dispersion force F_{TD} and wall lubrication force F_W is:

$$\vec{F}_{lg}=-\vec{F}_{gl}=\vec{F}_D+\vec{F}_L+\vec{F}_{TD}+\vec{F}_W \tag{8}$$

Modeling of interfacial drag force $\vec{F}_D$ calculated according to the Ishii-Zuber correlation. This model can be expressed as follows [17]:

$$\vec{F}_D=\left(\frac{3C_D}{4d_b}\right)\alpha_g \rho_l\left|U_g-U_l\right|\left(\vec{U}_g-\vec{U}_l\right) \tag{9}$$

Bubble diameter showing by d_b and the drag coefficient C_D depend on the flow regime. The lift force $\vec{F}_L$ is shear-induced and pushes the vapor bubbles towards the lower velocity region. The lift force on the liquid phase can be usually modeled as:

$$\vec{F}_L=C_L \alpha_g \rho_l\left(\vec{U}_g-\vec{U}_l\right)\times\left(\nabla\times\vec{U}_l\right) \tag{10}$$

The calculation was run by using the Tomiyama's model [18]. The lift force coefficient C_L depends on flow type, while for the viscous flow this value is between 0.01 and 0.11.
The effect of diffusion of vapor phase, caused by liquid phase turbulence, is described with turbulent dispersion force:

$$\vec{F}_{TD} = -C_{TD}\rho_l k \nabla \alpha_g \quad (11)$$

The liquid phase's turbulent kinetic energy indicates by k and C_{TD} denotes the turbulent dispersion coefficient, which was set to 0.1 according to Kurul and Podowski [8]. The wall lubrication force $\vec{F}_W$ acts in a lateral direction away from the wall and tends to push the vapor bubble away the heated wall. So, for computing the wall lubrication force we used the model of Antal et al. [19]:

$$\vec{F}_W = \alpha_g \rho_l \left(\frac{\left(\vec{U}_g - \vec{U}_l\right)^2}{d_b} \right) max\left(C_1 + C_2 \frac{d_b}{y_w},\ 0\right)\vec{n} \quad (12)$$

y_w denotes the distance to the nearest wall, In Eq. (12), n is the unit normal pointing away from the wall, C_1 and C_2 are −0.01 and 0.05 are the coefficients.
Because of the mechanical model on the subcooled boiling flow of Kurul and Podowski [8] the wall heat flux q_w is separated into three different components: the single-phase turbulent convection heat flux $q_{l\phi}$, the quenching heat flux q_Q and the wall evaporation heat flux q_e.

$$q_w = q_{l\varnothing} + q_e + q_Q = S_l \rho_l c_{pl} A_{l\varnothing} u_l \left(T_w - T_l\right) + 2f \left(\frac{\tau_Q \lambda_l \rho_l c_{pl}}{\pi} \right)^{0.5} A_{bub} \left(T_w - T_l\right) + \frac{N_a f \pi d_{bw}^3 \rho_g H_{lg}}{6} \quad (13)$$

The local Stanton number is denoted by S_l, and for the bubble nucleation frequency we have f, T_w is the wall temperature, T_l and u_l are the local liquid temperature and the liquid velocity at the first near-wall computational cell, respectively. The quenching period τ_Q between the departure of a bubble and the beginning of the growth of a subsequent one is defined as $0.8/f$. The area fraction influenced by the nucleating bubbles is A_{bub} and is usually formulated by $A_{bub}=min(1.\pi N_a d_{bw}^2)$, and the N_a is active nucleation sites density and d_{bw} is the bubble departure diameter. In addition, the remaining fraction $A_{l\varnothing}$1-A_{bub} is defined by the single-phase convection. For the active nucleation sites density N_a and the bubble nucleation frequency f and the following empirical correlations are applied (Koncar and Kljenak [14], Krepper et al. [20]).

$$N_a = \left(185\left(T_w - T_l\right)\right)^{1.085} \quad (14)$$

$$f = \sqrt{\frac{4g\left(\rho_l - \rho_g\right)}{\left(3d_{bw}\rho_l\right)}} \quad (15)$$

Many sub-models were close with bubble departure diameters, such as the bubble detachment frequency, evaporation heat flux, bubble area influence fraction and the bubble waiting time. Moreover, the bubble departure diameter is a crucial parameter in the wall heat flux partition model. d_W is modeled as a function of subcooling by Tolubinski and Kostanchuk [21].

$$d_{W(T)} = min\left(d_{ref} . \exp\left(-\frac{\Delta T_{sub}}{\Delta T_{ref}} \right). d_{max} \right) \quad (16)$$

The Eq. (14) parameters are dimensional (d_{ref}=0.6 mm, d_{max}=1.4 mm, ΔT_{sub}=45 K [22]) obtained from high-pressure water boiling experimental data. However, experimental data gathered by Unal [23], Zeitoun and Shoukri[24] , Bartel [22] and Prodanovic et al.[25] indicated that the bubble departure diameter d_W diverse with pressure conditions. In past studies, the Unal's model was proposed to describe the variation of bubble departure size along the heated wall for the low-pressure system. [23] Since equipment such as manifolds is working in low pressure condition, this method will not give admissible results for the bubble departure diameter. Fritz [26] introduced and presented a second departure diameter model for the low-pressure condition. The equation is:

$$d_{w(F)} = 0.208\ \varphi \sqrt{\frac{\sigma}{g\left(\rho_l - \rho_g\right)}} \quad (17)$$

The contact angle between the bubbles and the surface is φ [25]. So the results of this method are in better conditions with the experimental data than the Tolubinski [21] method. In addition, there is a lot of difference with the experimental results, which makes the Fritz's method uncertain for this project simulation.
Pressure, wall material, wall subheating, local liquid subcooling, etc. affect the departure bubble diameter. By using the initial inlet parameters, Unal formulated the bubble departure diameter correlation as follows [23]:

$$d_{w(U)} = \frac{(2.42)10^{-5}\,\mathrm{P}^{0.709}\mathrm{a}}{\sqrt{\mathrm{b}\Phi}} \quad (18)$$

where,

$$\mathrm{a} = \frac{\left(\mathrm{q_w} - \mathrm{h_{l\phi}}\Delta\mathrm{T_{sub}}\right)^{1/3}}{2\mathrm{C}^{1/3}\rho_\mathrm{g}\mathrm{H_{lg}}\sqrt{\pi \mathrm{k_l}/\rho_\mathrm{l}\mathrm{c_{pl}}}} \sqrt{\frac{\rho_\mathrm{s}\mathrm{c_{ps}}\mathrm{k_s}}{\mathrm{k_l}\rho_\mathrm{l}\mathrm{c_{pl}}}}$$

$$b = \frac{\Delta T_{sub}}{2\left(1 - \frac{\rho_g}{\rho_l}\right)} e^{\frac{\Delta T_{sub}}{2}} \quad if \quad \Delta T_{sub} \le 3K$$

$$b = \frac{\Delta T_{sub}}{2\left(1 - \frac{\rho_g}{\rho_l}\right)} \quad if \quad \Delta\mathrm{T_{sub}} > 3K$$

$$C = \frac{H_{lg}\mu_l \left[\frac{c_{pl}}{0.013 H_{lg} Pr_l^{1.7}} \right]^3}{\sqrt{\sigma/\left(\rho_g - \rho_l\right)g}}$$

$$\Phi = \max\left(\left(\frac{U_l}{U_o}\right)^{0.47}, 1\right)$$

U_l denotes the liquid velocity near the wall and u_0 0.61 m/s and our local pressure is P.

Phase changes of subcooled boiling flow are shown by the bubble evaporation on the heated wall and the bubble condensation in the bulk flow. The evaporation rate at wall per unit volume Γ_w can be obtained from evaporation heat flux q_e which can be calculated after the heat flux components calculation [27]:

$$\Gamma_w = \frac{q_e}{\lambda_{lg} + c_{pl}\Delta T_{sub}} \frac{A_i}{V_i} = \frac{N_a f\left(\frac{\pi}{6}\right) d_{bw}^3 \rho_g \lambda_{lg}}{\lambda_{lg} + c_{pl}\Delta T_{sub}} \frac{A_i}{V_i} \quad (19)$$

A_i and V_i denote the heat area and volume of i_{th} near the wall cell. The vapor bubbles may be surrounded by subcooled liquid and condense, after departure from the heated wall. Therefore, the rate of inter-phase heat transfer Q_{lg} and the interfacial condensation rate Γ_{cond} across the phase boundary per unit time per unit volume can be shown as [13]:

$$Q_{lg} = h_{lg} A_{lg} \left(T_{sat} - T_l\right) \quad (20)$$

$$\Gamma_{cond} = h_{lg} A_{lg} \left(T_{sat} - T_l\right) / H_{lg} \quad (21)$$

A_{lg} shows the interfacial area density, which can be denoted as $A_{lg}=6\alpha/d_b$, and h_{lg} is the liquid-interfacial heat transfer coefficient, describe as $h_{lg}=Nu_b\lambda_l/d_b$. The bubble Nusselt number Nu_b for a particle in a moving incompressible Newtonian fluid can be calculated from the Ranz-Marshall correlation [14]:

$$Nu_b = 2 + 0.6 Re_b^{0.5} Pr_l^{0.33} \quad (22)$$

So, Re_b is the bubble Reynolds and Pr_l is surrounding liquid Prandtl number.

3- Simulation

Designs of proposed configurations were performed in Solidworks. This manifold includes six inlets for hot gases from cylinders and an inlet with two outlets for coolant fluid. As shown in Fig. 3, based on the single channel proposed configuration, cooling water entered to the cooling passage with a mass flow rate of 6.1 kg per second and initial temperature of 333 K then it drains from the two outputs. As shown in Fig. 4, hot gases enter the manifold from 6 inputs at 1050 K with a mass flow rate of 1 kg per second and exit from the outlet.

The manifold body material is Cast Iron Alloy, which is not available in the software library. The Cast Iron Alloy properties were added to the software material library as shown in Table 1 [28].

Based on Fig. 5, meshing process was performed in ICEM CFD. Computational domain was divided into three parts including coolant fluid, manifold body and combustion gases. All the element type is tetrahedral and hexahedral in the maximum size of 6 mm.

Simulation of three configurations was performed using the computational fluid dynamics method in the ANSYS-CFX software. RPI boiling model, k-ω-SST turbulence model, and convection heat transfer for the outer surface of the body was applied as solver setting. As shown in Table 2, engine operating conditions were also applied to the input settings of the software. Convergence criterion is set as 1×10^{-4} and the residues of velocities, energy, and continuity are monitored accordingly.

Table 1. Cast iron material properties [28]

Parameters	Values
Molecular weight [kg/kmol]	50.57
Density [kg/m^3]	7150
Special heat capacity [J/kgK]	460
Conductivity heat transfer coefficient [W/mK]	48

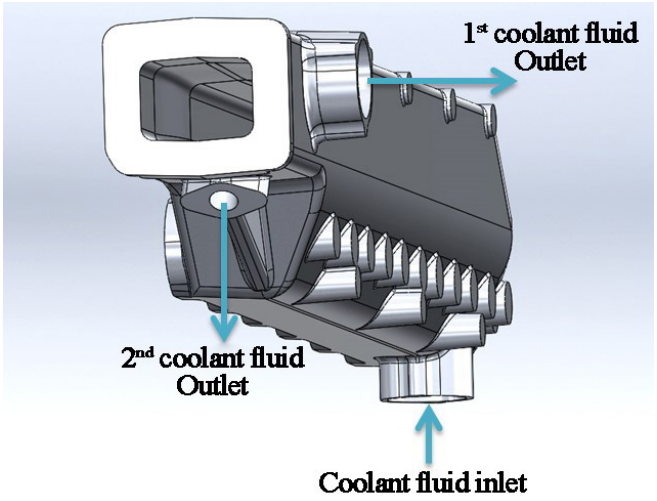

Fig. 3. Inlet and outlets of coolant

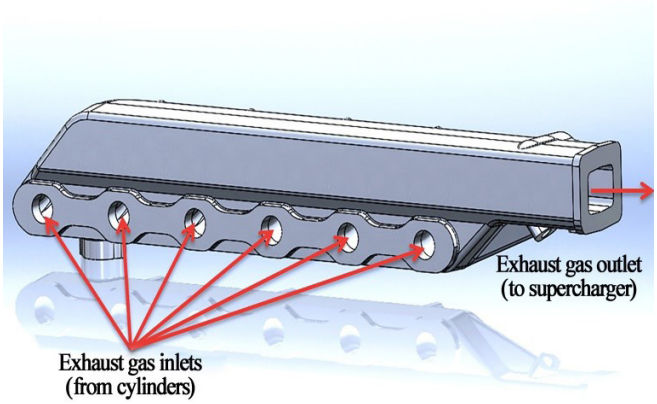

Fig. 4. Inlets and outlet of the exhaust gas

4- Grid Independence Analysis

To ensure the independence of the grid or mesh on the accuracy of the solution, the water temperature was considered at the coolant output. According to Table 3, the maximum size of elements is reduced to 7 and 6 mm and no changes in the results were obtained.

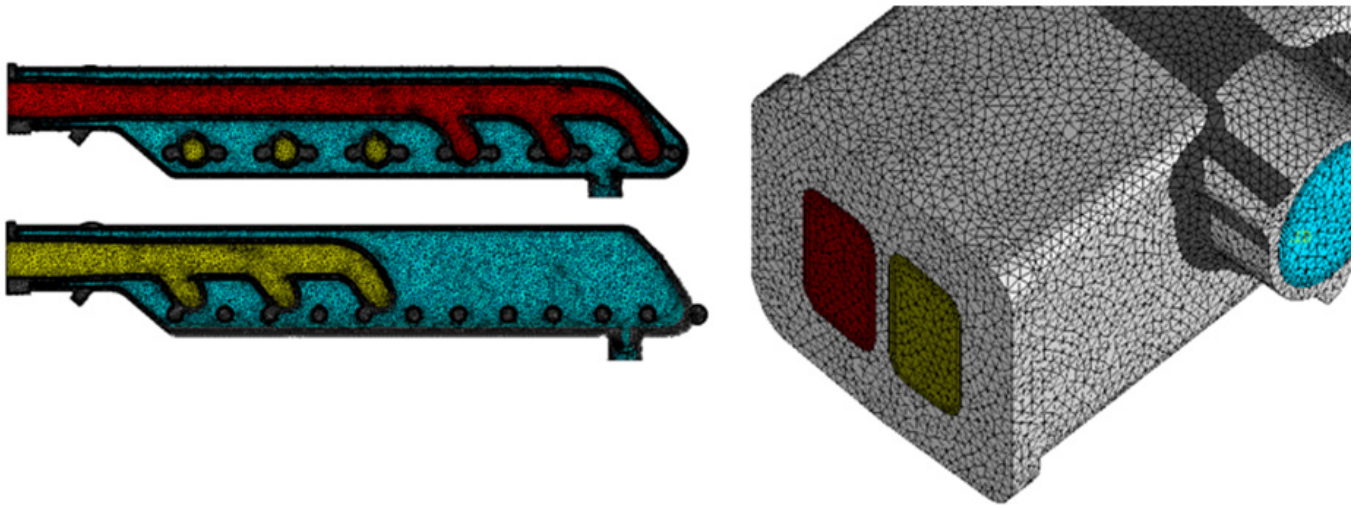

Fig. 5. Meshing

Table 2. Engine working condition

Parameters	Values
Engine speed (rpm)	2600
Combustion gas mass flow rate for each cylinder (kg/s)	1
Combustion gases temperature (K)	1050
Coolant mass flow rate (lit/s)	6.1
Coolant fluid temperature (K)	333

Table 3. Grid independence test

Maximum Element size (mm)	Water outlet temperature (°C)	Error (%)
12	71	19%
10	87	8%
8	82	3%
7	85	0%
6	85	0%

5- Validation

In this study, an approach has been taken to verify the accuracy of the simulation. The performance of the simulation in this work has been presented by comparing with the test results of body temperature under real working condition. Fig. 6 shows the temperature on the 6 parts where thermocouples were mounted in 200 mm distance to each other on the surface of the manifold shell. Simulation and measured temperature are shown in Table 4. The locations and values are depicted in the Fig. 6. As seen in the diagram, the results of test and simulation are well in agreement with each other and the maximum detected error is about 9 degrees (Fig. 6). This low difference is due to not considering parameters such as the effect of the cooling fluid fouling in its paths.

In addition, the coolant outlet temperature has been recorded as 353K. The results of simulation show this temperature is about 358K. Negligible 5 degrees temperature difference also verifies the accuracy of the simulation.

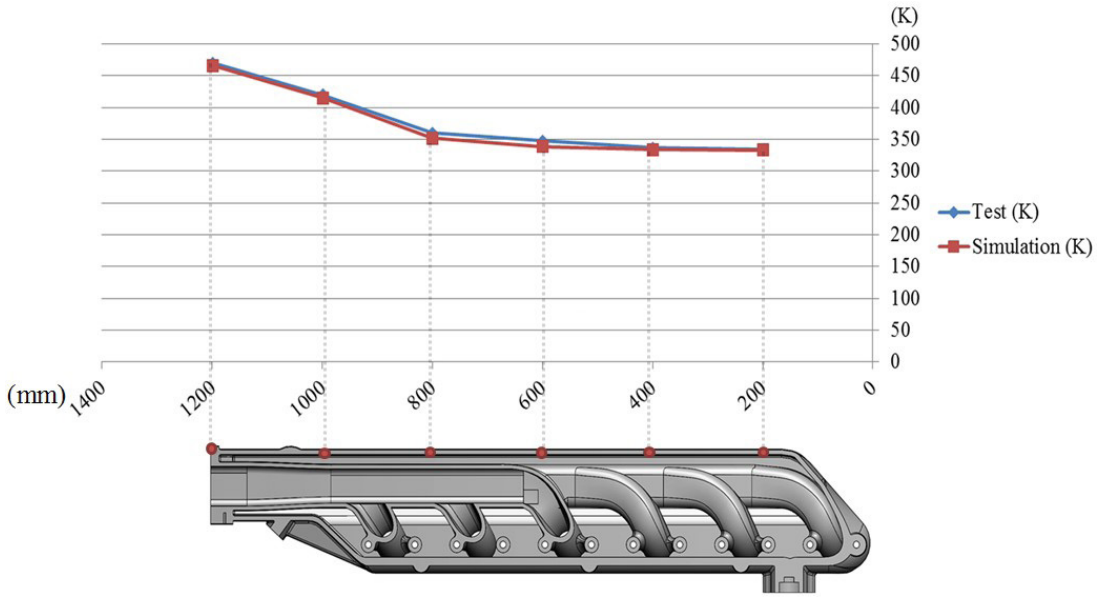

Fig. 6. Comparison between simulation and the measured temperature of shell surface

Table 4. Simulation and the measured temperature of the manifold shell surface

Distance (mm)	Simulation (K)	Experimental (K)
200	333	334
400	334	337
600	339	348
800	352	360
1000	415	420
1200	466	470

The highest level of accuracy in this study is related to the exact identification of the crack occurrence point in outlet separating wall. Comparing the result with simulation, which is presented in Fig. 7, confirms the validity of the simulation. Computational model validation already presented in previous research on primary geometry [6].

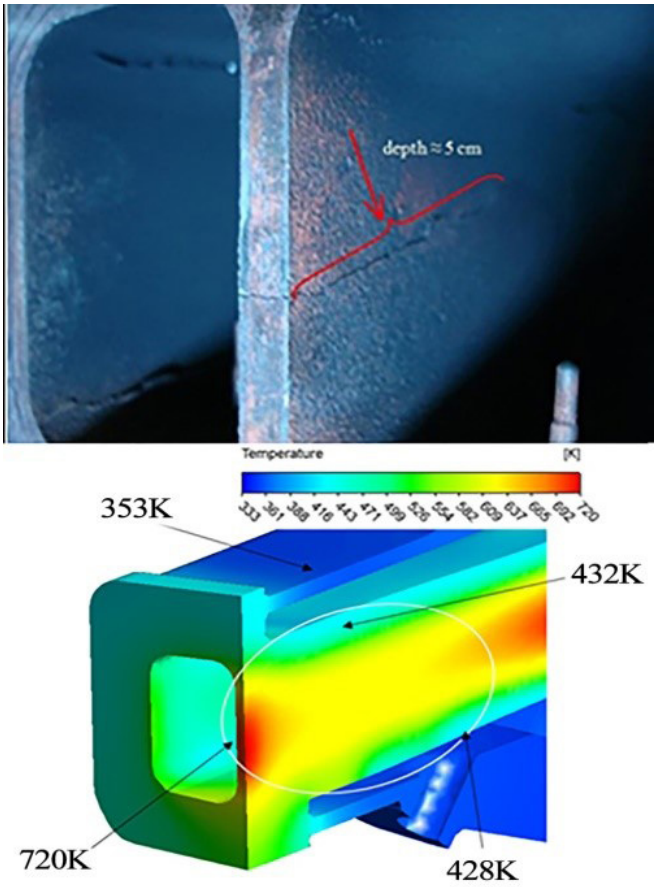

Fig. 7. In field test verified the location of crack the simulation

6- Results and Discussions

In cooling systems, the main goal is to achieve uniform thermal distribution in the domain to prevent hot and formation of extreme temperature gradients, which leads to the occurrence of phenomena resulting from thermal stresses such as crack. In the analysis of dual and single channel models, it was observed that the hot spots in the output section were well controlled. In the Primary geometry of manifold, the maximum temperature was 720 K at hot gases outlet (Fig. 8). Improvement of heat distribution in the proposed models

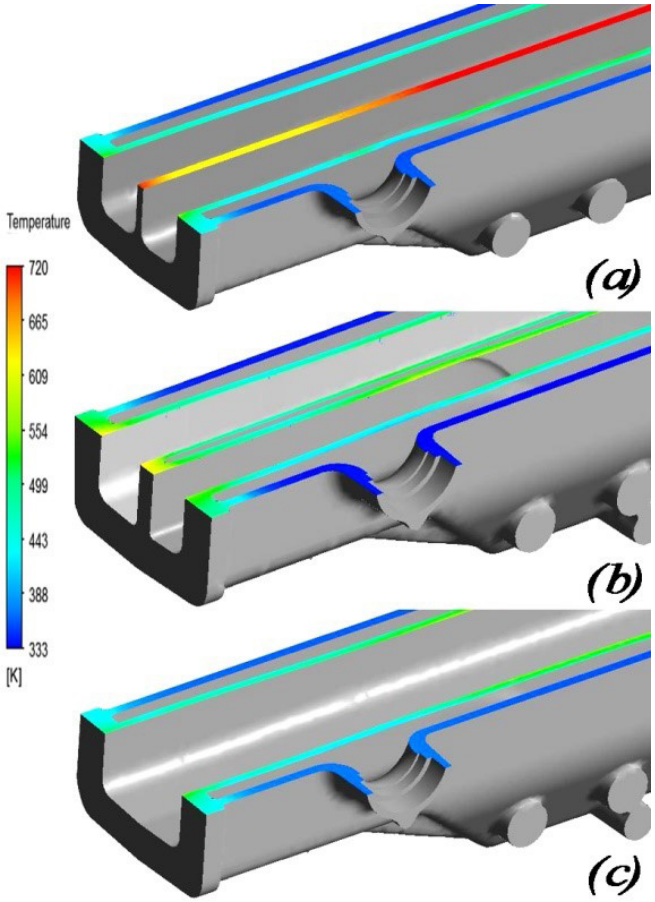

Fig. 8. Manifold body temperature distribution. (a) Primary configuration, (b) dual channel Geometry, (c) single channel configuration

is clearly visible. Contours of temperature can also identify a model with better Performance.

The dual channel configuration analysis, which is provided by creating a path for coolant fluid in output wall, shows this model cannot provide appropriate heat transfer and the maximum temperature dropped to 619 K it means that has fallen only 10 degrees. The single channel configuration analysis provided by removing the output-separating wall. Analysis of this Model shows, in addition to the correct operation of the manifold, reduces the temperature difference in the body and maximum temperature dropped to 523 K, which was a decrease of 197 degrees.

In Fig. 3, two outputs are shown for the coolant. Temperature distribution in the manifold body is depicted in Fig. 9. Examination of Fig. 3 and Fig. 9 can be concluded that the distance between the hot gases outlet wall and the coolant outlets causes an inappropriate non-uniform heat removal in this region. This problem becomes serious when the region with a maximum temperature of 720 K is in the vicinity of another part of the manifold which experiences 500 K temperatures. This difference in temperature causes thermal stresses and the main failure factor at this point of the body.

More uniform heat distribution can be noticed in the both proposed configurations (Fig. 9b and 9c), respectively, show the dual channel and single channel configuration of this study.

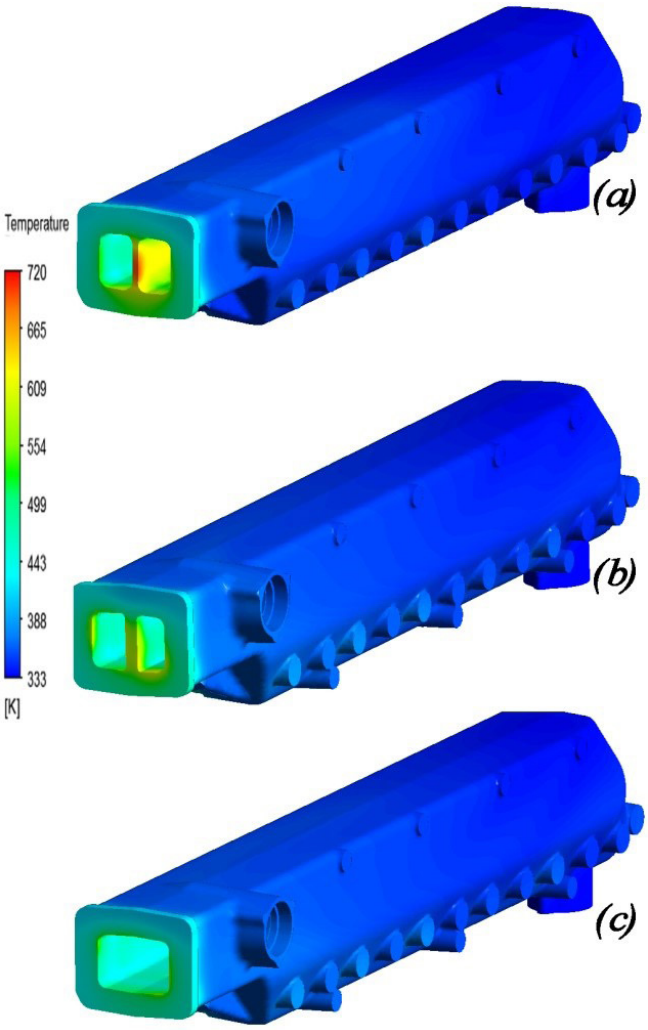

Fig. 9. Manifold body thermal distribution. . (a) Primary geometry, (b) dual channel configuration, (c) single channel configuration

Fig. 10 depicts the maximum temperature and hot spots on the body. For dual channel configuration at hot gas outlet area, the maximum temperature is 619 K. Temperature reduction about 100 degrees and up to 10% in hotspot verifying better efficiency in an alternative configuration. Nevertheless, the adjacent areas are at 323 K, which indicates 296 degree temperature difference in the manifold body. This should provide a solution to improve it.

Single channel configuration reduced the temperature difference to a significant level of 170 degrees. An overall design problem in the manifold body does not allow the temperature of the outlet side of the hot gases to be well controlled. Coolant outlets distance from the hot gas outlet wall causes inappropriate heat removal and higher temperature in this wall than the other parts of the body, even after modifications. The maximum body temperature was reduced up to 27.36%. Finally, Temperature reduction saved manifold body operation from critical conditions, extreme thermal gradients, and danger of crack occurrence. There is still need for more improvement.

7- Conclusions

Use of Computational fluid dynamics to resolve industrial problems is the fastest and least costly way for accurate examination and achieving an optimal design. In this study, it was shown that a slight change in geometry configuration, without changing the body material or new equipment utilize, can lead to better thermal gradients control. According to the manifold empirical investigation and industrial unit reports, the occurrence of crack cause coolant leakage to the combustion gases paths. Thus, the turbocharger and engine operation will be interrupted.

By using three-dimensional model, the numerical investigation of two-phase flow characteristics in subcooled boiling flow at low pressure in manifold coolant passages has been carried out; a new modified bubble departure diameter model for the low-pressure condition was performed based on the introduced model and correlation of others. This model was implemented by ANSYS-CFX software. An approach

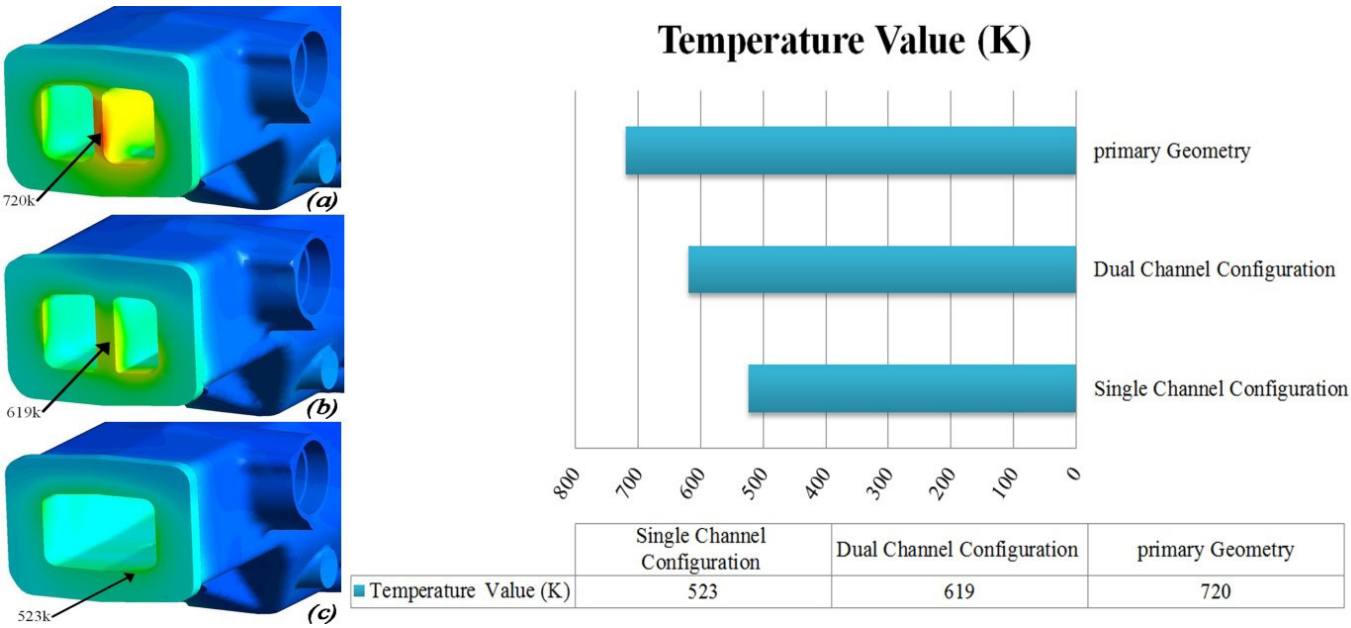

Fig. 10. The maximum body temperature. (a) Primary geometry, (b) dual channel configuration, (c) single channel configuration

has been taken to verify the accuracy of the numerical solving method. The most important results are:

- Creating a path for coolant fluid in the output wall as dual channel model, it shows despite better heat removal, this model cannot provide a uniform temperature distribution.
- Removing output separating wall as single channel model, without causing any problem in the passage of exhaust gases, eliminates the problem of creating hot spots and risk of crack occurrence, which is precisely the main goal of this study.
- Elimination of output separating wall provided more space for exhaust gases and better temperature distribution on manifold body.
- Thermal distribution results of the manifold body indicate a decrease in the maximum temperature up to 27.36% from 720 K to 523 K, which confirms the quality of the single channel proposed model as a suitable alternative to the initial geometry.
- Location of coolant fluid outlet is still one of the problems that should be considered in future researches.

Nomenclature

A_{bub}	wall fraction due to quenching, m^2
A_{lg}	interfacial area density
$A_{l\phi}$	single-phase convection area
C_{bw}	bubble departure coefficient
$C_{\mu b}$	coefficient in the Sato model of bubble induced turbulence
c_{pl}	liquid specific heat (J kg^{-1} K^{-1})
d_b	mean bubble diameter, m
d_{bw}	bubble departure diameter, m
f	bubble detachment frequency (s^{-1})
F	bubble force
$h_{l\phi}$	single-phase convection heat transfer coefficient (Wm^{-2} K^{-1})
h	heat transfer coefficient
$\vec{n}$	unit normal vector
Nu	Nusselt number
Nu_b	bubble Nusselt number
N_a	active nucleation site density
Pr_l	liquid Prandtl number
$q_{l\varphi}$	heat flux by single-phase convection, W
q_e	heat flux by evaporation, W
q_Q	heat flux by quenching, W
q_w	wall heat flux, W/m^2
Q_{lg}	interfacial heat transfer rate, W/m^2
Re_b	bubble Reynolds number
St	Stanton number
T	temperature
u	Velocity, m/s
RPI	Rensselaer Polytechnic Institute

Greek symbol

α	volume fraction
ρ	Density, kg/m^3
ε	eddy dissipation rate
Γ_{Cond}	interfacial condensation rate
Γ	mass transfer ($kg.s^{-1}.m^{-3}$)
μ	dynamic viscosity, kg/m.s
μ^{eff}	effective viscosity
μ_l^{turb}	Turbulence viscosity
μ_l^b	bubble-induced turbulence viscosity
ν	kinematic viscosity, m^2/s
σ	surface tension coefficient, N/m^2

Subscripts

l	liquid
g	vapor
ref	Reference value
sat	saturation
sub	subcooling
w	wall

References

[1] J.B. Heywood, O.Z. Welling, Trends in performance characteristics of modern automobile SI and diesel engines, *SAE International Journal of Engines*, 2(1) (2009) 1650-1662.

[2] H. Punekar, S. Das, Numerical simulation of subcooled nucleate boiling in cooling jacket of IC engine, 0148-7191, *SAE Technical Paper*, 2013.

[3] C. Karl, U. Feldhaus, CFD simulation for the cooling circuit of a truck diesel engine, *MTZ worldwide*, 69(2) (2008) 12-19.

[4] R. Van Basshuysen, U. Spicher, *Gasoline engine with direct injection: processes, systems, development, potential, Vieweg+ Teubner*, 2009.

[5] N. Kanawade, O. Siras, Design, analysis, and development of 4-cylinder IC engine exhaust manifold, *International Engineering Research Journal*, (2015) 472-478.

[6] M. Asari, S. Adeli, P. Nikandish, Thermal and fluid flow analysis for diesel engine exhaust manifold with regard to the boiling phenomenon and compare with experimental results, *AJSR-ME*, 50(4) (2018) 21-30.

[7] R. Bowring, W. Idsinga, N. Todreas, An assessment of two-phase pressure drop correlations for steam-water systems, *International Journal of Multiphase Flow* 3(5) (1977) 401-413.

[8] M.Z. Podowski, N. Kurul, On the modeling of multidimensional effects in boiling channels, in: 27th *National Heat Transfer Conference*, Minneapolis, Minnesota, USA, 1991.

[9] A.P. Shingare, N.B. Totla, Simulation of Jacket Cooling of a Liner of Four Cylinder Diesel Engine for Genset Application, *International Engineering Research Journal* (*IERJ*), (2016) 276-1283,.

[10] V.A. Romanov, N.A. Khozeniuk, Experience of the diesel engine cooling system simulation, *Procedia Engineering*, 150 (2016) 490-496.

[11] A. Mohammadi, M. Yaghoubi, Two phase flow simulation for subcooled nucleat boiling heat transfer calculation in water jacket of diesel engine, *Journal of Engine Research*, (2011).

[12] A.V. Paratwar, D.B. Hulwan, Surface temperature prediction and thermal analysis of cylinder head in diesel engine, *IJERA*, 3(4) (2013) 892-902.

[13] E. Chen, Y. Li, X. Cheng, L. Wang, Modeling of low-pressure subcooled boiling flow of water via the homogeneous MUSIG approach, *Nuclear Engineering Design*, 239(10) (2009) 1733-1743.

[14] B. Končar, I. Kljenak, B. Mavko, Modelling of local two-phase flow parameters in upward subcooled flow boiling at low pressure, *International Journal of Heat Mass Transfer*, 47(6-7) (2004) 1499-1513.

[15] ANSYS, ANSYS-CFX theory guide - Multiphase Flow Theory, 2006.

[16] Y. Sato, M. Sadatomi, K. Sekoguchi, Momentum and heat transfer in two-phase bubble flow—I. Theory, *International Journal of Multiphase Flow*, 7(2) (1981) 167-177.

[17] M. Ishii, N. Zuber, Drag coefficient and relative velocity in bubbly, droplet or particulate flows, *AIChE Journal* 25(5) (1979) 843-855.

[18] A. Tomiyama, Struggle with computational bubble dynamics, *Multiphase Science Technology*, 10(4) (1998) 369-405.

[19] S.P. Antal, R.T. Lahey Jr, J.E. Flaherty, Analysis of phase distribution in fully developed laminar bubbly two-phase flow, *International Journal of Multiphase Flow*, 17(5) (1991) 635-652.

[20] E. Krepper, B. Končar, Y. Egorov, CFD modelling of subcooled boiling—concept, validation and application to fuel assembly design, *Nuclear Engineering Design*, 237(7) (2007) 716-731.

[21] V. Tolubinsky, D. Kostanchuk, Vapour bubbles growth rate and heat transfer intensity at subcooled water boiling, in: *International Heat Transfer Conference*, Begel House Inc., Paris, France, 1970.

[22] M.D. Bartel, *Experimental investigation of subcooled boiling*, Purdue University, WestLafayette, USA, 1999.

[23] H.C. Ünal, Maximum bubble diameter, maximum bubble-growth time and bubble-growth rate during the subcooled nucleate flow boiling of water up to 17.7 MN/m^2, 19(6) (1976) 643-649.

[24] O. Zeitoun, M. Shoukri, Bubble behavior and mean diameter in subcooled flow boiling, *ASME journal of Heat Transfer*, 118(1) (1996) 110-116.

[25] V. Prodanovic, D. Fraser, M. Salcudean, Bubble behavior in subcooled flow boiling of water at low pressures and low flow rates, *International Journal of Multiphase Flow*, 28(1) (2002) 1-19.

[26] W. Fritz, Berechnung des maximalvolumes von dampfblasen, *Physik. Zeitschr*, 36 (1935) 379-384.

[27] S. Hua, R. Huang, P. Zhou, Numerical investigation of two-phase flow characteristics of subcooled boiling in IC engine cooling passages using a new 3D two-fluid model, *Applied Thermal Engineering*, 90 (2015) 648-663.

[28] H.T. Angus, *Cast iron: physical and engineering properties*, Elsevier, London, 2013.

Please cite this article using:

M.R. Assari, S. Adeli, A. Ebn-Abbas, New Design and Analysis of Diesel Exhaust Manifold to Control Thermal Gradient, *AUT J. Mech. Eng.*, 3(1) (2019) 53-62.

DOI: 10.22060/ajme.2018.14440.5729